journal of the mechanical behavior of biomedical materials 160 (2024) 106749

Contents lists available at ScienceDirect

Journal of the Mechanical Behavior of Biomedical Materials

journal homepage: www.elsevier.com/locate/jmbbm

Research paper

Anisotropic swelling due to hydration constrains anisotropic elasticity in biomaterial fibers

Xander A. Gouws, Ana Mastnak, Laurent Kreplak, Andrew D. Rutenberg *

Department of Physics and Atmospheric Science, Dalhousie University, Halifax, B3H 4R2, Nova Scotia, Canada

ARTICLE INFO

Keywords:
Hydration
Anisotropic swelling
Anisotropic elasticity
Collagen fibrils
Hair fiber
Poisson ratio

ABSTRACT

Naturally occurring protein fibers often undergo anisotropic swelling when hydrated. Within a tendon, a hydrated collagen fibril's radius expands by 40% but its length only increases by 5%. The same effect, with a similar relative magnitude, is observed for single hair shafts. Fiber hydration is known to affect elastic properties. Here we show that *anisotropic* swelling constrains the anisotropic linear elastic properties of fibers. First we show, using data from disparate previously reported studies, that anisotropic swelling can be described as an approximately linear function of water content. Then, under the observation that the elastic energy of swelling can be minimized by the anisotropic shape, we relate swelling anisotropy to elastic anisotropy — assuming radial (transverse) symmetry within a cylindrical geometry. We find an upper bound for the commonly measured axial Poisson ratio $\nu_{zx} < 1/2$. This is significantly below recently estimated values for collagen fibrils extracted from tissue-level measurements, but is consistent with both single hair shaft and single collagen fibril mechanical and hydration studies. Using ν_{zx}, we can then constrain the product $\gamma \equiv (1-\nu_{xy})E_z/E_x$ — where ν_{xy} is the seldom measured transverse Poisson ratio and E_z/E_x is the ratio of axial to radial Young's moduli.

1. Introduction

Many biomaterials absorb water in response to changes in the ambient humidity. Leonardo da Vinci used this effect to make the first hygrometer, or humidity sensor, in 1481 using the changing mass of cotton with humidity. In 1783, hair hygrometers were developed that used the changing length of hair shafts with humidity (Korotcenkov, 2019), and were widely used until the last century. More generally, any biomaterial or biotextile will have changing water content with humidity (see, e.g., Yin et al., 2023). The increasing development and use of biomaterials and biotextiles makes the systematic effects of hydration important to characterize.

For relatively well-studied biological fibers, such as hair shafts and collagen fibrils, the effects of hydration are dramatic. Mechanical properties of hair shafts depend strongly on water content (Popescu and Höcker, 2007), as do modes of mechanical failure (Kamath and Weigmann, 1982). The Young's modulus of collagen fibrils varies by orders of magnitude between dry and aqueous conditions (Andriotis et al., 2018); similar scale changes are seen in bending (Yang et al., 2008) or indentation (Andriotis et al., 2018; Grant et al., 2008) and in keratin appendages (Johnson et al., 2017). Furthermore, mechanical effects of hydrated fibers are strongly affected by solution conditions — reflecting different water contents (Grant et al., 2009; Masic et al., 2015; Haverkamp et al., 2022).

Both hair shafts and collagen fibrils are strongly anisotropic materials, with fibril-forming alpha-keratins or fibril-forming collagen molecules predominantly aligned with the cylindrical axis of individual hair shafts or collagen fibrils, respectively. Substantial anisotropy is also observed with hydration effects. When hydrated, a collagen fibril's radius may expand by 40% while its length only increases by 5% (Haverkamp et al., 2022). Similarly, when a hair shaft is hydrated, its radius expands by 14%, but its length expands by only 2% (White and Eyring, 1947; Stam et al., 1952).

Substantial elastic anisotropy is also observed in these systems. Studies of single collagen fibrils exhibit ratios of axial to radial stiffness greater than 20 (Andriotis et al., 2018, 2023). A study of human hair shafts shows stiffness ratios as large as 2 (Breakspear et al., 2018). How this mechanical anisotropy may relate to the swelling anisotropy has not been examined, though both swelling and mechanical anisotropies should ultimately arise from the anisotropic structures of these biomaterial fibers.

Our goal in this paper is to simplify, summarize, and compare the anisotropic phenomenology due to hydration in both hair and collagen fibers. Since the water content of protein fibers can vary by osmolarity

* Corresponding author.
E-mail address: adr@dal.ca (A.D. Rutenberg).

https://doi.org/10.1016/j.jmbbm.2024.106749
Received 4 July 2024; Received in revised form 8 August 2024; Accepted 14 September 2024
Available online 17 September 2024

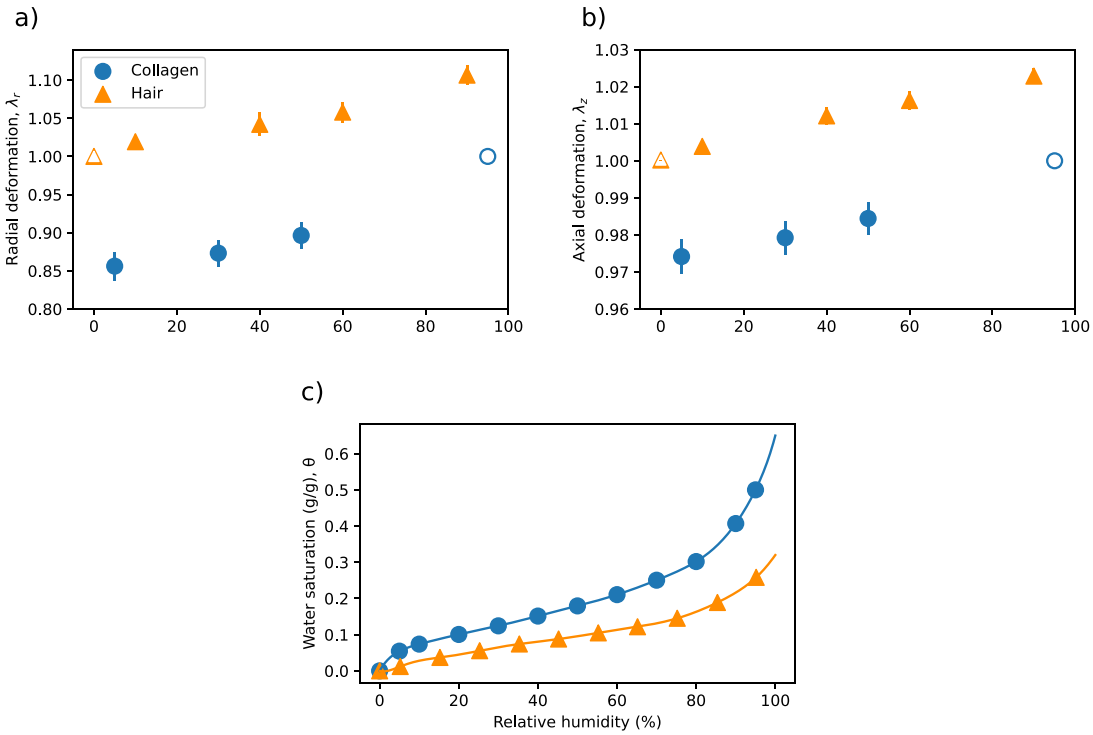

Fig. 1. Previously reported hydration data. (a) radial deformation of hair shafts ("hair") (Stam et al., 1952) and collagen fibrils ("collagen") (Masic et al., 2015), (b) axial deformation of hair (Stam et al., 1952) and collagen (Masic et al., 2015), (c) water saturation (g water/g material) for hair (Barba et al., 2010) and collagen (Bull, 1944), with interpolating lines fit using the Guggenheim–Anderson–de Boer (GAB) model from Barba et al. (2010). For hair, the hydration curve is shown. All are vs. relative humidity (%). Standard errors are indicated. Unfilled points indicate the baseline states.

even at a fixed relative humidity (Grant et al., 2009; Masic et al., 2015; Haverkamp et al., 2022), we investigate how shape depends on water content. We obtain a simple phenomenological model for this relationship. We use this model to constrain anisotropic linear elastic models — independently of any microscopic structural model. Since these elastic models are coarse-grained, we also obtain an effective coarse-grained mechanism for anisotropic swelling in biomaterial fibers. We expect this elastic picture of swelling to generically apply for small strains, where linear elasticity applies.

2. Methods and results

Relative dimensional changes induced by variations in relative humidity have been previously experimentally characterized. We have extracted digitized collagen fibril data (Masic et al., 2015), and used raw hair shaft hydration measurements (Stam et al., 1952). Fig. 1a shows the radial deformation

$$\lambda_r = R/R_0, \tag{1}$$

for both collagen fibrils ("collagen", blue circles in all figures) and hair shafts ("hair", orange triangles) vs. relative humidity, where R is the cylindrical radius and R_0 is the baseline radius at the relative humidity indicated by the unfilled points. All error bars in this paper are standard errors of the means ("standard errors"), corresponding to one standard deviation. Fig. 1b shows the corresponding axial deformations

$$\lambda_z = L/L_0, \tag{2}$$

where L is the axial length and L_0 is the baseline length.

We are interested in how the water content of hair and collagen affects their shapes and structures. Independent studies have examined the relationship between water content and humidity both in hair (Barba et al., 2010) and in collagen (Bull, 1944), as shown in Fig. 1c. These experiments report saturation θ as the grams of water absorbed per gram of protein dry mass. Errors were not reported for

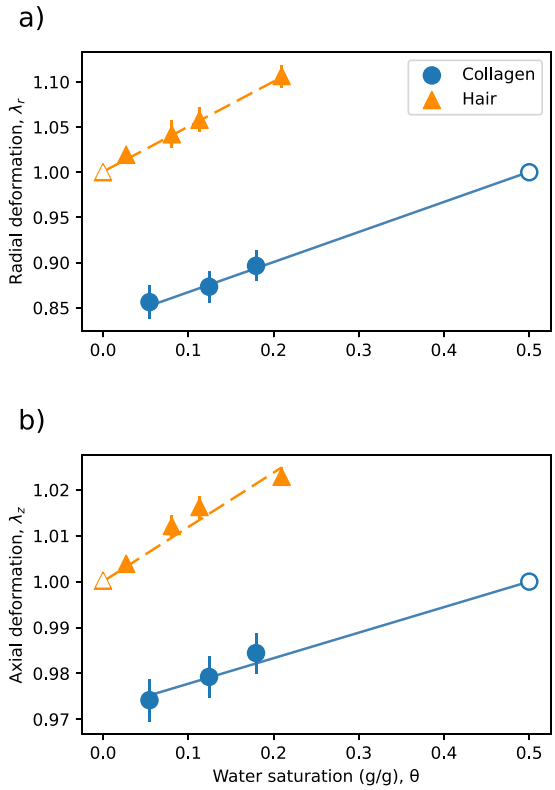

Fig. 2. Deformations vs. water saturation using the data from Fig. 1. (a) Radial deformation, λ_r vs. saturation θ (grams of water absorbed per gram of dry mass). (b) Axial deformation λ_z vs. θ. Unfilled points indicate the baseline states. Colored lines are linearized from fits in Fig. 3.

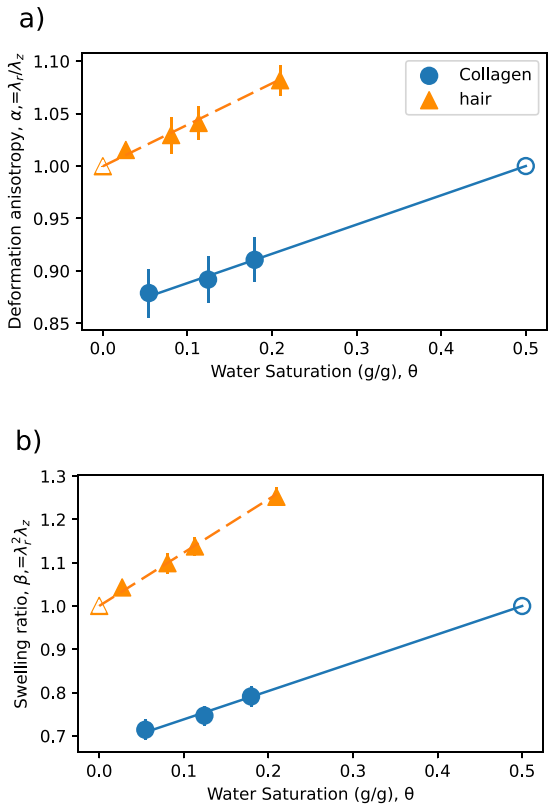

Fig. 3. Geometric deformations vs. water saturation. (a) Deformation anisotropy $\alpha = \lambda_r/\lambda_z$ vs. saturation θ. (b) Swelling ratio $\beta = \lambda_r^2\lambda_z$ vs. θ. Lines are linear best fits.

these saturation studies. How deformations change with saturation θ has not been previously reported, but can be extracted by using the deformation studies exploring ambient humidity (Stam et al., 1952; Masic et al., 2015).

The experimental data used here (Stam et al., 1952; Masic et al., 2015; Barba et al., 2010; Bull, 1944) are from different groups, with different samples, and with different techniques. For the hair swelling studies (Stam et al., 1952), human hair strands with dry diameters between 40–60 μm and with cross-sectional elliptical eccentricity less than 1.1 were used. For the hair water content studies (Barba et al., 2010), untreated human hair was used. For the collagen water content studies (Bull, 1944), non-fibrillar collagen extracted from 'hide' was used. For the collagen swelling studies (Masic et al., 2015), radial and axial strain of fibrils during swelling was extracted from X-ray studies of unstressed rat tail tendon. These experiments have not been quantitatively replicated by other groups and do not include estimates of systematic errors, so that the errors shown may represent underestimates of the actual experimental errors.

In Fig. 2, we re-plot the deformation data from Fig. 1 as a function of saturation. We have interpolated the saturation data of hair as needed, using the theoretical function given by Barba et al. (2010) and shown in Fig. 1c. Note that the hair study used a dehydrated baseline (at $\theta_0 \approx 0$) and explored the effects of increased hydration while the collagen study used a hydrated baseline ($\theta_0 \approx 0.5$) and then dehydrated the samples. We see that the deformations vary approximately linearly with saturation. Since $\lambda \approx 1$, deformations to any low power are also approximately linear with respect to saturation.

To investigate how shape changes with water content, we define the deformation anisotropy

$$\alpha \equiv \lambda_r/\lambda_z, \tag{3}$$

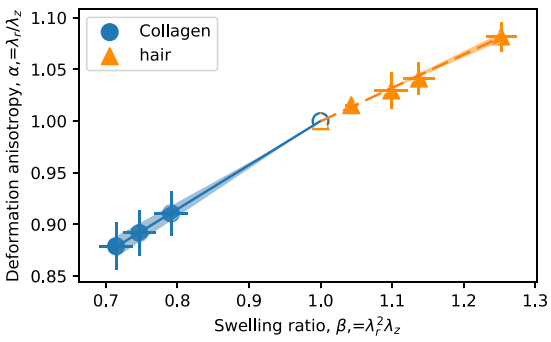

Fig. 4. Deformation anisotropy $\alpha = \lambda_r/\lambda_z$ vs. swelling ratio $\beta = \lambda_r^2\lambda_z = V/V_0$, for both hair and collagen as indicated. Unfilled points indicate the baseline state at $\alpha_0 = \beta_0 = 1$. The lines are linear best-fits, while the shaded regions indicate standard errors of the fit.

which is a measure of how anisotropic the deformations are. We also define a geometric measure of water content, the swelling ratio

$$\beta \equiv \lambda_r^2\lambda_z = V/V_0, \tag{4}$$

which is how much the volume (V) has changed with respect to the baseline volume (V_0). Our phenomenological model is that both α and β are linear functions of the saturation θ (i.e. the water content):

$$\alpha = 1 + A(\theta - \theta_0) \tag{5}$$

and

$$\beta = 1 + B(\theta - \theta_0). \tag{6}$$

The initial saturation θ_0 is the saturation at which the baseline lengths R_0 and L_0 have been measured, where $\lambda = \alpha = \beta = 1$. We generically expect $B > 0$ if added water leads to added volume, but we have no such constraint on A.

In Fig. 3, α and β have been plotted as functions of the saturation together with best-fit lines from our linear model Eqs. (5) and (6). For hair and collagen, the best-fit slope parameters are

$$A_{\text{collagen}} = 0.28 \pm 0.03, \tag{7}$$

$$B_{\text{collagen}} = 0.65 \pm 0.06, \tag{8}$$

$$A_{\text{hair}} = 0.40 \pm 0.05, \text{ and} \tag{9}$$

$$B_{\text{hair}} = 1.23 \pm 0.08, \tag{10}$$

where errors are standard errors (representing one standard deviation). These parameters have been determined using Deming regression with the *SciPy* version 1.13.1 orthogonal distance regression subpackage. With no errors in θ, this performs ordinary least squares fitting whilst accounting for uncertainty in the data.

We can plot $\alpha(\theta)$ and $\beta(\theta)$ against each other as a parametric function of the saturation θ. This is shown in Fig. 4. Since the baseline point at $\alpha_0 = \beta_0 = 1$ must be shared, we expect from Eqs. (5) and (6) that

$$\alpha - 1 = m(\beta - 1), \tag{11}$$

where m is a slope parameter. While we have $m = A/B$, we refit m to estimate standard errors using Deming regression. We obtain:

$$m_{\text{collagen}} = 0.43 \pm 0.04, \text{ and} \tag{12}$$

$$m_{\text{hair}} = 0.32 \pm 0.03. \tag{13}$$

Values of A and B let us (at leading order in θ) estimate $\lambda_r \simeq 1 + (\theta - \theta_0)(A + B)/3$ and $\lambda_z \simeq 1 + (\theta - \theta_0)(B - 2A)/3$. These estimates are shown as straight lines in Fig. 2. Note that since we expect that λ_z grows with water content (along with λ_r), we should have $B > 2A$ and so $m \simeq A/B < 1/2$ — as observed.

3. Anisotropic elasticity

Linear elastic theory allows us to explore the relationship between anisotropic swelling and anisotropic elastic properties for small volume changes. For a given water content (swelling ratio β), we will determine the anisotropic shape ratio α that minimizes the elastic strain energy. We will use this to relate m to anisotropic elasticity.

Taking fibers as transversely isotropic orthotropic materials, the compliance matrix relating strain and stress is (Slaughter, 2002)

$$\begin{bmatrix}\varepsilon_{xx}\\ \varepsilon_{yy}\\ \varepsilon_{zz}\end{bmatrix} = \begin{bmatrix}1/E_x & -\nu_{yx}/E_y & -\nu_{zx}/E_z\\ -\nu_{xy}/E_x & 1/E_y & -\nu_{zy}/E_z\\ -\nu_{xz}/E_x & -\nu_{yz}/E_y & 1/E_z\end{bmatrix}\begin{bmatrix}\sigma_{xx}\\ \sigma_{yy}\\ \sigma_{zz}\end{bmatrix}, \tag{14}$$

where we have assumed zero shear. This relates the strains ε_{ii} to the stresses σ_{ii} through the Young's moduli E_i and Poisson ratios ν_{ij}, where the axial (longitudinal) direction is z and the symmetric radial directions are x and y. Using this radial symmetry, we have $E_x = E_y$, $\varepsilon_{xx} = \varepsilon_{yy}$, $\sigma_{xx} = \sigma_{yy}$, $\nu_{xy} = \nu_{yx}$, and $\nu_{xz} = \nu_{yz}$. Since the compliance matrix is also symmetric, we further have $\nu_{zx}/E_z = \nu_{xz}/E_x$. As a result, there are only four independent elastic parameters that are relevant: E_x, E_z, ν_{xy}, and ν_{zx}.

Taking advantage of symmetries, and inverting the resulting 2×2 matrix, we obtain

$$\begin{bmatrix}\sigma_{xx}\\ \sigma_{zz}\end{bmatrix} = \frac{1}{1-\nu_{xy}-2\nu_{xz}\nu_{zx}}\begin{bmatrix}E_x & \nu_{zx}E_x\\ 2\nu_{zx}E_x & (1-\nu_{xy})E_z\end{bmatrix}\begin{bmatrix}\varepsilon_{xx}\\ \varepsilon_{zz}\end{bmatrix}. \tag{15}$$

For small strains, the elastic strain energy density is

$$u = \frac{1}{2}\left(\varepsilon_{xx}\sigma_{xx}+\varepsilon_{yy}\sigma_{yy}+\varepsilon_{zz}\sigma_{zz}\right) = \varepsilon_{xx}\sigma_{xx}+\frac{1}{2}\varepsilon_{zz}\sigma_{zz}. \tag{16}$$

Using Eq. (15) this gives

$$u = \frac{1}{1-\nu_{xy}-2\nu_{xz}\nu_{zx}}\left[E_x\varepsilon_{xx}^2+2\nu_{zx}E_x\varepsilon_{xx}\varepsilon_{zz}+\frac{1}{2}(1-\nu_{xy})E_z\varepsilon_{zz}^2\right]. \tag{17}$$

Taking small $\hat{\alpha}\equiv\alpha-1\simeq\varepsilon_{xx}-\varepsilon_{zz}$ and $\hat{\beta}\equiv\beta-1\simeq 2\varepsilon_{xx}+\varepsilon_{zz}$, we can take $\varepsilon_{xx}\simeq(\hat{\alpha}+\hat{\beta})/3$ and $\varepsilon_{zz}\simeq(\hat{\beta}-2\hat{\alpha})/3$. This allows us to easily minimize u with respect to $\hat{\alpha}$ (keeping $\hat{\beta}$ fixed) to obtain

$$\alpha-1\simeq m(\beta-1) \tag{18}$$

where

$$m = \frac{(1-\nu_{xy})E_z/E_x-(1-\nu_{zx})}{2(1-\nu_{xy})E_z/E_x+(1-4\nu_{zx})}. \tag{19}$$

If the elasticity is isotropic (with $E_z/E_x = 1$ and $\nu_{xy} = \nu_{zx}$) then the swelling is too ($m = 0$) — so that the observation of swelling anisotropy ($m > 0$) implies elastic anisotropy.

We can re-express m in terms of two parameters

$$m = \frac{1}{2}+\frac{3(\nu_{zx}-1/2)}{2(\gamma-2\nu_{zx}^2)+(2\nu_{zx}-1)^2}, \tag{20}$$

where $\gamma\equiv(1-\nu_{xy})E_z/E_x$. For elastic stability we need $u > 0$ in Eq. (17), which implies $1-\nu_{xy}-2\nu_{zx}\nu_{xz} > 0$ (Eqn. 11 of Lempriere (1968)). From the symmetric compliance we have $\nu_{zx}/E_z = \nu_{xz}/E_x$, which then gives $\gamma > 2\nu_{zx}^2$. As a result, the denominator in Eq. (20) must be strictly positive. From the previous section we expect, and observe, that the slope $m < 1/2$. This implies that the axial Poisson ratio $\nu_{zx} < 1/2$.

Typically, ν_{zx} is directly measured in uniaxial extension experiments (see Discussion). Solving for the unknown γ in Eq. (20) we then have

$$\gamma = \frac{1}{2}+\frac{1+4m}{1-2m}\left(\frac{1}{2}-\nu_{zx}\right). \tag{21}$$

Since we expect $\nu_{zx} < 1/2$ and $m < 1/2$, we then also expect $\gamma > 1/2$. This satisfies the stability requirement $\gamma > 2\nu_{zx}^2$ when $\nu_{zx} < 1/2$.

4. Discussion

We have parameterized the relationship between water content and anisotropic swelling in two protein fibers — hair shafts and collagen fibrils. We have shown that available experimental data exhibits an approximately linear dependence between shape measures and the water content, with remarkably similar behavior between hair shafts and collagen fibrils. A plot of the strain anisotropy ϵ_r/ϵ_z (where $\epsilon = \lambda-1$) highlights the large ~5-fold strain anisotropies that are observed (Fig. 5). It also highlights the considerable experimental uncertainty that remains.

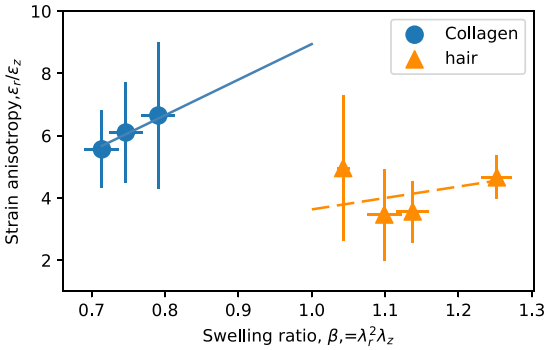

Fig. 5. Strain anisotropy vs. swelling ratio. Using the same data as Fig. 4, we plot the strain anisotropy ϵ_r/ϵ_z vs. the swelling ratio $\beta = \lambda_r^2\lambda_z = V/V_0$ — for both hair and collagen as indicated. Note that $\epsilon = \lambda-1$. The lines assume Eqs. (5)–(6) together with the exact fit values of A and B.

We have connected the anisotropic swelling to anisotropic elasticity, under the assumption that swelling due to hydration chooses an anisotropic shape that minimizes the elastic energy. Our results constrain the elastic constants. From assuming that increasing water increases both the radial and axial deformations, we expect that $m < 1/2$ — which we observe. This in turn constrains the well-measured axial Poisson's ratio $\nu_{zx} < 1/2$. These additionally constrain the product $\gamma\equiv(1-\nu_{xy})E_z/E_x > 1/2$ — which also satisfies elastic stability. While ν_{xy} has not been measured, ν_{zx} has been.

For hair shafts, $\nu_{zx} = 0.37\pm0.05$ (Lee and Kwon, 2013), and using $m_{\text{hair}} = 0.32\pm0.03$ we estimate that $\gamma_{\text{hair}} = 1.3\pm0.4$. This satisfies $\gamma > 1/2$. With the further assumption that neither hair shafts nor collagen fibrils are radially auxetic (i.e. that $\nu_{xy}\geq 0$) we expect that $E_z/E_x\geq\gamma$ i.e. $E_z/E_x\geq 1.3\pm0.4$ in hair. The mechanical anisotropy of hair shafts has been recently measured (Breakspear et al., 2018), albeit the analysis assumed $\nu_{xy} = 1/2$. For hair cortex, they found $E_z/E_x\simeq 1.95$ at small relative humidity (Breakspear et al., 2018) — in agreement with our bound. Though the uncertainties are large, we can use this to crudely estimate $\nu_{xy} = 1-\gamma/(E_z/E_x)\approx 0.33$ for dry hair. Increased precision of the experiments could improve and constrain this estimate.

For collagen, recent X-ray studies of bovine pericardial tissue estimated $\nu_{zx} = 2.1\pm0.7$ (Wells et al., 2015). A similar value ($\nu_{xz}\approx 1.9$) can be extracted from AFM studies of tendon (Rigozzi et al., 2013; Wells et al., 2015). These substantially violate our bound $\nu_{zx} < 1/2$. However, both of these studies involved estimates of fibril properties from tissue — which likely violates the transversely isotropic symmetry assumed in our treatment. Studies of individual (isolated from rat tail tendon) collagen fibrils instead report $\nu_{zx}\approx 0$ (see e.g. Fig. S11a of Peacock and Kreplak (2019)) — which satisfies our bound. Using $\nu_{zx} = 0$, we estimate $\gamma\simeq 10$, and we bound $E_z/E_x\geq 10$. Brillouin scattering experiments have estimated the elastic anisotropy of wet collagen tissue and extracted $E_z/E_x\approx 1.8$ (Cusack and Miller, 1979) — recent measurements of dry collagen tissue obtain all elastic constants and a similar small ratio (Edginton et al., 2016). In contrast, mechanical study of individual collagen fibrils has determined both $E_x\approx 15\,\text{MPa}$ by AFM nanoindentation and $E_z\approx 0.4\,\text{GPa}-0.8\,\text{GPa}$ by AFM tensile tests (Andriotis et al., 2018, 2023) — resulting in $E_z/E_x\approx 27-54$, consistent with our bounds. We can use these to estimate $\nu_{xy} = 1-\gamma/(E_z/E_x)\approx 0.6-0.8$ from single-fibril studies.

Both hair shafts and collagen fibrils have anisotropic structures with similar anisotropic response to hydration (see Fig. 4). Nevertheless,

the microscopic mechanisms for this response is thought to differ. For collagen fibrils, axial deformations are thought to be minimized by the sliding of collagen molecules past each other (Haverkamp et al., 2022). In contrast, intermediate filaments in hair shafts do not themselves restructure by sliding, but rather they guide the anisotropic swelling of the surrounding amorphous matrix (Robbins, 2008; Murthy et al., 2019). These different microstructural models should, in principle, lead to different anisotropic properties of these materials — as is seen in our estimates of the elastic parameters.

Elastic parameters vary with humidity and hence water content (see e.g. Breakspear et al., 2018) — consistent with the enormous differences between hydrated and dry samples (see e.g. Andriotis et al., 2023). For hair, the elastic anisotropy E_z/E_x decreases with increasing water content to ≃0.9 (Breakspear et al., 2018). Our elasticity treatment applies for small (linear) deformations with respect to any reference water content, and so should still apply if we take $d\alpha \simeq m\, d\beta$ in Eq. (18), for small changes $d\alpha$ and $d\beta$. In other words $m = d\alpha/d\beta$, the local slope in Fig. 4. From $m < 1/2$, we also expect the slope $d\alpha/d\beta < 1/2$. From Eq. (21) the slope determines the combination $\gamma = (1 - \nu_{xy})E_z/E_x$, but presumably ν_{xy} is also hydration dependent in hair. The approximate linearity of α vs. β in Fig. 4 indicates that the net hydration dependence of γ may not be strong in either hair or collagen.

We expect that our results would also apply to other anisotropic biomaterials, biomimetic materials, and synthetic materials. For example, Mredha et al. (2017) created a millimeter diameter biomimetic "hair" by crosslinking a water soluble polymer solution containing aligned collagen fibrils. They achieved hydrogels with axial deformations after hydration that ranged from 1.04 to 1.29, and radial deformations from 1.18 to 1.7. Despite using very different chemistries from hair, all formulations showed significant swelling strain anisotropy between 2 and 5. Our results indicate that considerable elastic anisotropy would be expected as well.

We have assumed a straight and radially symmetric geometry, which is not generically true for hair shafts (Wolfram, 2003). In particular curly hair has asymmetric structure in cross-section (Thibaut et al., 2007), as with wool (Munro and Carnaby, 1999). Hair is also approximately elliptical in cross section (Wolfram, 2003), though the data we have used is from hair with small cross-sectional eccentricity (Stam et al., 1952). The structural complexity (inhomogeneity) of single hair shafts (Wolfram, 2003) may also lead to more complex behavior. These variations would complicate our mechanical analysis, and presumably also swelling behavior, though probably in interesting ways. Whether water content controlled by solution conditions (see e.g. Grant et al., 2009; Masic et al., 2015; Haverkamp et al., 2022) or cross-linking density (see e.g. Miles et al., 2005; Andriotis et al., 2019; Vaez et al., 2023) has the same phenomenology as water content controlled by humidity also remains an open question experimentally, since our swelling results are based on studies that have only varied relative humidity.

We have shown how linear anisotropic hydration would be related to linear anisotropic elasticity given our symmetry assumptions. Previous studies of hair shafts and collagen fibrils should be systematically revisited to validate how shape and mechanical properties depend on humidity and water content. Similar studies for other isolated biomaterial fibers would also test and extend our results.

CRediT authorship contribution statement

Xander A. Gouws: Writing – review & editing, Writing – original draft, Visualization, Software, Methodology, Investigation, Formal analysis, Data curation, Conceptualization. **Ana Mastnak:** Visualization, Investigation, Data curation. **Laurent Kreplak:** Writing – review & editing, Supervision, Conceptualization. **Andrew D. Rutenberg:** Writing – review & editing, Supervision, Project administration, Funding acquisition, Formal analysis, Conceptualization.

Declaration of competing interest

The authors declare that they have no known competing financial interests or personal relationships that could have appeared to influence the work reported in this paper.

Data availability

The authors do not have permission to share data.

Acknowledgments

We thank the Natural Sciences and Engineering Research Council of Canada (NSERC) for operating Grants RGPIN-2024-04192 (LK) and RGPIN-2019-05888 (ADR).

References

Andriotis, O.G., Desissaire, S., Thurner, P.J., 2018. Collagen fibrils: Nature's highly tunable nonlinear springs. ACS Nano 12 (4), 3671–3680. http://dx.doi.org/10.1021/acsnano.8b00837.

Andriotis, O.G., Elsayad, K., Smart, D.E., Nalbach, M., Davies, D.E., Thurner, P.J., 2019. Hydration and nanomechanical changes in collagen fibrils bearing advanced glycation end-products. Biomed. Opt. Express 10 (4), 1841. http://dx.doi.org/10.1364/boe.10.001841.

Andriotis, O.G., Nalbach, M., Thurner, P.J., 2023. Mechanics of isolated individual collagen fibrils. Acta Biomater. 163, 35–49. http://dx.doi.org/10.1016/j.actbio.2022.12.008.

Barba, C., Martí, M., Manich, A., Carilla, J., Parra, J., Coderch, L., 2010. Water absorption/desorption of human hair and nails. Thermochim. Acta 503–504, 33. http://dx.doi.org/10.1016/j.tca.2010.03.004.

Breakspear, S., Noecker, B., Popescu, C., 2018. Hair mechanical anisotropy-what does it tell us? J. Cosmet. Sci. 69 (5), 305–314.

Bull, H.B., 1944. Adsorption of water vapor by proteins. J. Am. Chem. Soc. 66, 1499. http://dx.doi.org/10.1021/ja01237a025.

Cusack, S., Miller, A., 1979. Determination of the elastic constants of collagen by Brillouin light scattering. J. Mol. Biol. 135 (1), 39–51. http://dx.doi.org/10.1016/0022-2836(79)90339-5.

Edginton, R.S., Mattana, S., Caponi, S., Fioretto, D., Green, E., Winlove, C.P., Palombo, F., 2016. Preparation of extracellular matrix protein fibers for Brillouin spectroscopy. J. Vis. Exp.: JoVE (115), 54648. http://dx.doi.org/10.3791/54648.

Grant, C.A., Brockwell, D.J., Radford, S.E., Thomson, N.H., 2008. Effects of hydration on the mechanical response of individual collagen fibrils. Appl. Phys. Lett. 92 (23), 233902. http://dx.doi.org/10.1063/1.2937001.

Grant, C.A., Brockwell, D.J., Radford, S.E., Thomson, N.H., 2009. Tuning the elastic modulus of hydrated collagen fibrils. Biophys. J. 97 (11), 2985–2992. http://dx.doi.org/10.1016/j.bpj.2009.09.010.

Haverkamp, R.G., Sizeland, K.H., Wells, H.C., Kamma-Lorger, C., 2022. Collagen dehydration. Int. J. Biiol. Macromol. 216, 140–147. http://dx.doi.org/10.1016/j.ijbiomac.2022.06.180.

Johnson, K., Trim, M., Francis, D., Whittington, W., Miller, J., Bennett, C., Horstemeyer, M., 2017. Moisture, anisotropy, stress state, and strain rate effects on bighorn sheep horn keratin mechanical properties. Acta Biomater. 48, 300–308. http://dx.doi.org/10.1016/j.actbio.2016.10.033.

Kamath, Y.K., Weigmann, H.-D., 1982. Fractography of human hair. J. Appl. Polym. Sci. 27 (10), 3809–3833. http://dx.doi.org/10.1002/app.1982.070271016.

Korotcenkov, G., 2019. Handbook of Humidity Measurement, Methods, Materials and Technologies. Vol. 2, pp. 23–29. http://dx.doi.org/10.1201/b22370-3, Ch. Mechanical (hair) hygrometer.

Lee, J., Kwon, H.J., 2013. Measurement of stress–strain behaviour of human hair fibres using optical techniques. Int. J. Cosmet. Sci. 35 (3), 238–243. http://dx.doi.org/10.1111/ics.12031.

Lempriere, B.M., 1968. Poisson's ratio in orthotropic materials.. AIAA J. 6 (11), 2226–2227. http://dx.doi.org/10.2514/3.4974.

Masic, A., Bertinetti, L., Schuetz, R., Chang, S.-W., Metzger, T.H., Buehler, M.J., Fratzl, P., 2015. Osmotic pressure induced tensile forces in tendon collagen. Nature Commun. 6 (1), 5942. http://dx.doi.org/10.1038/ncomms6942.

Miles, C.A., Avery, N.C., Rodin, V.V., Bailey, A.J., 2005. The increase in denaturation temperature following cross-linking of collagen is caused by dehydration of the fibres. J. Mol. Biol. 346 (2), 551–556. http://dx.doi.org/10.1016/j.jmb.2004.12.001.

Mredha, M.T.I., Kitamura, N., Nonoyama, T., Wada, S., Goto, K., Zhang, X., Nakajima, T., Kurokawa, T., Takagi, Y., Yasuda, K., Gong, J.P., 2017. Anisotropic tough double network hydrogel from fish collagen and its spontaneous in-vivo bonding to bone. Biomaterials 132, 85–95. http://dx.doi.org/10.1016/j.biomaterials.2017.04.005.

Munro, W.A., Carnaby, G.A., 1999. Wool-fibre crimp part I: The effects of microfibrillar geometry. J. Text. Inst. 90 (2), 123–136. http://dx.doi.org/10.1080/00405009908690618.

Murthy, N.S., Wang, W., Kamath, Y., 2019. Structure of intermediate filament assembly in hair deduced from hydration studies using small-angle neutron scattering. J. Struct. Biol. 206 (3), 295–304. http://dx.doi.org/10.1016/j.jsb.2019.04.004.

Peacock, C.J., Kreplak, L., 2019. Nanomechanical mapping of single collagen fibrils under tension. Nanoscale 11 (30), 14417–14425. http://dx.doi.org/10.1039/c9nr02644d.

Popescu, C., Höcker, H., 2007. Hair—the most sophisticated biological composite material. Chem. Soc. Rev. 36 (8), 1282–1291. http://dx.doi.org/10.1039/b604537p.

Rigozzi, S., Müller, R., Stemmer, A., Snedeker, J., 2013. Tendon glycosaminoglycan proteoglycan sidechains promote collagen fibril sliding—AFM observations at the nanoscale. J. Biomech. 46 (4), 813–818. http://dx.doi.org/10.1016/j.jbiomech.2012.11.017.

Robbins, C.R., 2008. Chemical and Physical Behavior of Human Hair. Springer, Berlin, Heidelberg.

Slaughter, W.S., 2002. The Linearized Theory of Elasticity. Springer Science+Business Media, LLC.

Stam, P.B., Kratz, R.F., White, H.J., 1952. The swelling of human hair in water and water vapor. Text. Res. J. 22 (7), 448–465. http://dx.doi.org/10.1177/004051755202200702.

Thibaut, S., Barbarat, P., Leroy, F., Bernard, B.A., 2007. Human hair keratin network and curvature. Int. J. Dermatol. 46 (s1), 7–10. http://dx.doi.org/10.1111/j.1365-4632.2007.03454.x.

Vaez, M., Asgari, M., Hirvonen, L., Bakir, G., Khattignavong, E., Ezzo, M., Aguayo, S., Schuh, C.M., Gough, K., Bozec, L., 2023. Modulation of the biophysical and biochemical properties of collagen by glycation for tissue engineering applications. Acta Biomater. 155, 182–198. http://dx.doi.org/10.1016/j.actbio.2022.11.033.

Wells, H.C., Sizeland, K.H., Kayed, H.R., Kirby, N., Hawley, A., Mudie, S.T., Haverkamp, R.G., 2015. Poisson's ratio of collagen fibrils measured by small angle X-ray of strained bovine pericardium. J. Appl. Phys. 117 (4), 044701. http://dx.doi.org/10.1063/1.4906325.

White, H.J., Eyring, H., 1947. Textile research journal. Text. Res. J. 17 (10), 523–553. http://dx.doi.org/10.1177/004051754701701001.

Wolfram, L.J., 2003. Human hair: A unique physicochemical composite. J. Am. Acad. Dermatol. 48 (6), S106–S114. http://dx.doi.org/10.1067/mjd.2003.276.

Yang, L., Werf, K.O.v.d., Fitié, C.F., Bennink, M.L., Dijkstra, P.J., Feijen, J., 2008. Mechanical properties of native and cross-linked type I collagen fibrils. Biophys. J. 94 (6), 2204–2211. http://dx.doi.org/10.1529/biophysj.107.111013.

Yin, J., Li, J., Reddy, V.S., Ji, D., Ramakrishna, S., Xu, L., 2023. Flexible textile-based sweat sensors for wearable applications. Biosensors 13 (1), 127. http://dx.doi.org/10.3390/bios13010127.